A method for optimising the arrangement of internal channels in aircraft hydraulic manifolds manufactured by additive manufacturing

Dingbo Li[1], Haixiang Huang[1], Xiaochao Liu[1,*], Peiyao Hou[1] & Honghui Liao[2]

[1] School of Automation Science and Electrical Engineering, Beihang University, Beijing 100191, China
[2] Large Aircraft Advanced Training Center, Beihang University, Beijing, PR China

Abstract

Selective Laser Melting (SLM), a type of 3D printing technology, is used to rapidly manufacture complex parts by melting selected areas of material layer by layer. Aircraft hydraulic manifolds can be machined using SLM to achieve small size, low resistance, and high machining quality simultaneously. Therefore, it is necessary to investigate a method for the design of internal channels for additive manufacturing of aircraft hydraulic manifolds. In this paper, a novel optimisation method for the alignment of the channels is proposed. It is based on the A-star algorithm, which integrates volume, resistance, and surface quality. The channel is first parameterised in terms of centre line coordinates and channel diameter. Then, the channel resistance coefficient model and the forming surface roughness model are established through experiments. Meanwhile, a cost function including centreline length, channel resistance and surface roughness is built and embedded into the A-star algorithm, and then the centreline is smoothed using mean filtering. It is worth mentioning here that engineers can adjust the coefficients in the cost function to obtain the optimal channel arrangement scheme according to the actual demand. The results show that the planning method proposed in this paper can obtain the channel arrangement scheme with short path, low resistance, and low surface roughness.

Keywords: Aircraft hydraulic manifold; Selective laser melting; A-star algorithm; Channel arrangement scheme

1. Introduction

The aerospace complex hydraulic manifold is a device that facilitates the connection of hydraulic system piping to hydraulic components, which achieves compact cartridge integration of multiple hydraulic components through the intricate internal runner structure. It is one of the hydraulic components with the largest number of uses, the most complex runner layout, and the greatest weight reduction potential in aviation hydraulic systems. The utilisation of traditional material reduction manufacturing methods, such as drilling, boring, milling, chipping, etc., can result in the formation of a considerable number of right-angle turning pipelines, process hole cavities and other structures. These structures, however, are associated with a few inherent disadvantages, including increased flow resistance, the inability to remove the excess dead weight and an increased volume. Selective Laser Melting (SLM) can be employed to rapidly manufacture round turning pipelines, no process cavity pipelines, gradient diameter pipelines, and other shaped pipelines [1,2], which provides a novel approach to reducing volume and enhancing internal fluid performance. Consequently, investigating the potential of SLM for aircraft hydraulic manifold internal runner arrangement and design offers considerable scope for future applications.

In recent years, several companies have produced 3D-printed hydraulic manifolds for specific applications. Materials Solutions[3] has created a high-performance aerospace hydraulic manifold using titanium alloys, which meets the most stringent requirements of aircraft. Chemnitz University of Technology and Liebherr Group[4] designed and manufactured a 3D-printed hydraulic manifold for the A380's spoiler actuator, which was flight-proven on the A380. Renishaw[5] has enhanced the functionality of the 3D-printed hydraulic manifold by 60% through a continuous process of design optimisation. Although various companies and educational institutions have produced 3D-printed hydraulic manifolds, there is still considerable scope for their structural optimisation. In parallel with

the development of computer technology, numerous design software packages for hydraulic manifolds have been developed. The University of Bath[6] has developed a software program, VOLE, which can automatically design a 3D model of the hydraulic integrated piping network. This model can then be used to visualize the flow situation of the internal runners of the integrated block. Chambon et al.[7] have developed a more intelligent runner design software by integrating AI design and CAD principles into the design of runners. In addition, several scholars [8-10] believe that experimental measurements and numerical simulations are effective methods for evaluating pipeline structures.

This paper presents a novel multi-dimensional runner alignment optimisation method based on the improved A-star algorithm,which includes a multi-objective function in three dimensions, namely runner length, local resistance and surface roughness. In this paper, multiple spherical barriers are employed to equate the hydraulic components, and the requisite safety distance between the runner and the hydraulic components is guaranteed by expanding the spherical barriers.This method not only achieves simultaneous optimisation of multidirectional flow paths, but also generates a piping network consisting of multiple outlets and inlets in series. In this paper, this optimisation method is used to optimise the internal flow path arrangement of an aircraft hydraulic manifold. The results demonstrate that the method not only effectively removes additional structures such as blind cavities and process holes, but also reduces the pressure loss by more than 60%.

2. Problem description

Current aircraft hydraulic manifolds are mainly shaped by conventional machining. Consequently, when developing the internal runners of aircraft hydraulic manifolds, it is not only essential to create the runners in conventional shapes such as 'Z'-shaped pipes, right-angle turning pipes and stepped pipes, but also to incorporate additional structures such as process holes and blind cavities, as illustrated in Fig. 1. Nevertheless, SLM technology enables the formation of shaped lines, including circular turn lines and B-spline lines, which can not only reduce the volume and weight of the aircraft hydraulic manifold, but also minimise pressure loss. Consequently, the utilisation of SLM technology to manufacture aircraft hydraulic manifolds represents a prospective development trend in the field of aviation manufacturing. The enhanced degree of freedom afforded by SLM technology for aircraft hydraulic manifold runner arrangement renders traditional runner arrangement and design methods obsolete. It is necessary to propose a method for SLM aircraft hydraulic manifolds that can both improve the fluid performance and reduce the size of the piping network.

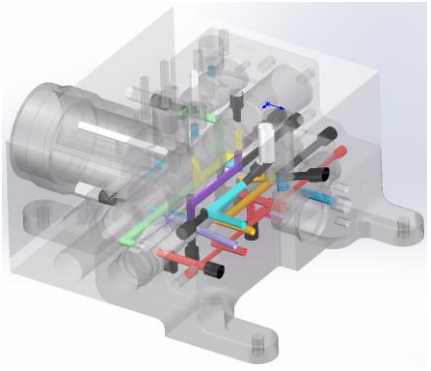

Figure 1 – Aircraft hydraulic manifold need to be optimised.

3. Theoretical and Methodological

3.1 A-star Algorithm Description

The A-star algorithm is a heuristic search algorithm that is commonly employed to identify the shortest path in graphical networks. It integrates the benefits of the breadth-first search of Dijkstra's algorithm and the greedy best-first search, enabling the search range to be narrowed as much as possible while ensuring that the shortest path is identified, thereby enhancing the search efficiency. The fundamental principle is to select the next node by evaluating the cost function of each node.The cost function for each node of the A-star algorithm is presented in Equation 1. As can be observed from the formula, the cost function is comprised of two components: the actual cost and the heuristic

function. The actual cost is employed to calculate the cost from the starting point to the current node. The heuristic function is utilized to estimate the cost from the current node to the target node. In the algorithm, the cost is typically interpreted as the distance required to achieve the goal of the shortest path. By considering both costs together, the A-star algorithm selects the node with the lowest total cost, thereby ensuring that the path generated by its final optimisation is the optimal solution.

$$F(n)=G(n)+H(n) \tag{1}$$

Where G(n) is the cost function from the starting point to the current node and H(n) is the cost function from the current node to the goal point.

The A-star algorithm is a path search algorithm utilising rasters. Therefore, it is necessary to define the objective space and cost function prior to its utilisation. During the execution of the algorithm, two lists are generated: The Openlist and Closelist are two lists that are generated by the A-star algorithm. The Openlist contains the nodes that have been visited but not selected as the next node. The Closelist contains the nodes that have not been visited or have not been expanded after being visited. The nodes that have already been explored are placed into the Openlist by the A-star algorithm. The evaluation function is used to rank the nodes in the Openlist, with the objective of identifying the optimal nodes for traversal. The nodes are evaluated and selected based on their proximity to the optimal nodes, with the goal of generating the path with the minimum surrogate value. The algorithmic implementation process is as follows:

(1) Set up Openlist and Closelist, Openlist to hold nodes that have been searched and Closelist to hold nodes that have not been explored.

(2) Set X as the initial raster point and Y as the specified target point. Place the initial raster point in Openlist.

(3) The nodes in the vicinity of the initial raster point are visited. Non-obstacle points are placed in the Openlist, and their valuation distances are calculated using a heuristic function. The initial raster point is then placed in the Closelist.

(4) The next expansion point N is placed in Closelist according to the optimal selection strategy. If N is the specified target raster, the path planning is completed and the algorithm runs successfully. Otherwise, the following steps are performed.

(5) The strategy of accessing its surrounding nodes is continued for the raster N. For the surrounding child nodes that are not included in the Closelist, they are added to the Openlist for the purpose of cost computation.

(6) The algorithm was found to be successful in running, with the map and extension nodes being saved, and the backtracking connection representing the final path.

From Equation 1, it can be seen that when G(n)>> H(n), F(n)≈G(n). This indicates that the A-star algorithm is equivalent to Dijkstra's algorithm, and that the number of search nodes will be increased, which will result in an increase in the search time. Furthermore, when G(n)<< H(n), F(n)≈H(n). In this case, the A-star algorithm is equivalent to the BFS algorithm, with the search becoming more efficient but with the potential for local optimal solutions to emerge. Consequently, the impact of the H(n) function on whether it constitutes an optimal path in the A-star algorithm is of great significance. The most used heuristic functions include Euclidean distance and Manhattan distance. Given that the computational accuracy of the Euclidean distance is superior to that of the Manhattan distance, the Euclidean distance is selected as the heuristic function in this paper. To illustrate, if the coordinates of the two points are (x_1, y_1) and (x_2, y_2), the heuristic function H(n) can be expressed as:

$$H(n)=\sqrt{(x_1-x_2)^2+(y_1-y_2)^2} \tag{2}$$

The A-star algorithm employs a raster map to represent the environmental information within the hydraulic integration block. The final optimised path generated is the centreline of the flow path. This paper presents the construction of this algorithm, which was completed using MATLAB, and simulation tests were carried out, as shown in Figure 2. When utilising this optimisation algorithm, the initial and target positions and obstacles can be defined within the raster map. The simulation map of the A-star algorithm is represented as a spatial raster map, with green dots indicating the initial position points, blue round dots denoting pipeline exits, raster spheres representing obstacles, red connecting lines denoting final paths, and coloured dots signifying searched points. The final generated path exhibits considerable curvature, which will result in elevated flow resistance. In this

paper, the path is subjected to a smoothing process via mean filtering, as illustrated in Fig. 2.

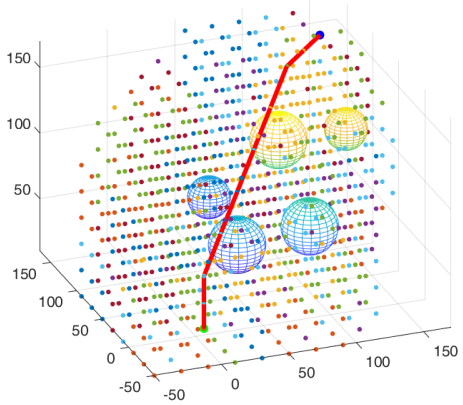

Figure 2 – Implementation of A-star algorithm path planning.

3.2 Obstacle design

During the design of a flow path, obstacles such as cartridge components can be present within the hydraulic integrated block. Obstacle avoidance can be effectively achieved by the A-star algorithm. However, before obstacle avoidance is implemented, obstacle design should be carried out first. This involves the irregular cartridge components being equivalently designed as regular shaped obstacles. In the context of flow channel design, the conventional obstacle design methodology involves importing the actual cartridge element model for data preprocessing. This enables the model section processing to be carried out, which yields the data information pertaining to the cross-section of each layer. This approach ensures that there is a high degree of accuracy between the imported model and the real model. In comparison to the process of importing the actual cartridge element for model slicing, the model of the actual cartridge element represented by a simple 3D model is more computationally efficient and has less impact on the final flow path design. In this study, the components inserted in the hydraulic block are equivalent to cylinders, which are then wrapped by multiple spheres and expanded to ensure that the runners have a certain safe distance from the components, as illustrated in the figure below.

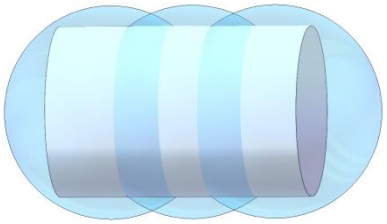

Figure 3 – Obstacle equivalent design.

Fig. 4 illustrates the geometric relationship between the barrier sphere following the expansion treatment and the hydraulic element. The cylindrical shape represents the equivalent hydraulic element, with its top intersecting the sphere. All three red vertices in the figure are located on the sphere and form a circular cross-section. From the geometrical relationship illustrated in Fig. 4:

$$\begin{cases} \dfrac{h_2}{h_1} = k \\ k = \dfrac{R-r}{R-\sqrt{R^2-r^2}} \\ h = \sqrt{R^2-r^2} \end{cases} \tag{3}$$

Where R and r represent the radius of the sphere and the cylinder, respectively. h denotes the distance from the centre of the sphere to the bottom of the cylinder, h1 is the distance from the bottom of the cylinder to the surface of the sphere, and h2 is the distance from the side of the cylinder to the surface of the sphere. Engineers can modify the values of k and h by adjusting the radius of

the sphere R in accordance with the specific requirements of the barrier sphere. In this project, an aerospace hydraulic integrated block is used as an example for the optimisation of the internal runner arrangement, setting $R=\sqrt{2}r$.

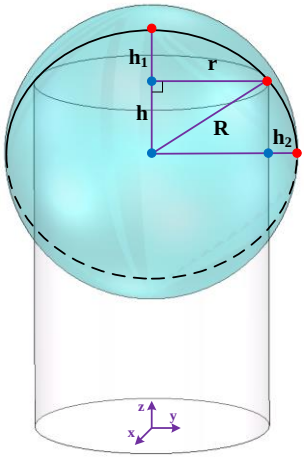

Figure 4 – Scheme of equivalent barrier geometry.

3.3 Cost function improvement

The advantages of A-star algorithm are high search efficiency, simple computation, and globally optimal solution. However, the paths planned by the A-star algorithm tend to have more inflection points, which may not be suitable for the internal runner arrangement of the integrated block. Therefore, improvements may be necessary in the application. When using the A-star algorithm to optimally generate the centreline of the runner, it is necessary to modify the cost function of the nodes. In this paper, two additional items, M(n) and R(n), are incorporated into the original G(n) and H(n), as illustrated in the following equation:

$$F(n)=k_1 \bullet G(n)+k_2 \bullet H(n)+k_3 \bullet M(n)+k_4 \bullet R(n) \tag{4}$$

Where the coefficients k_1, k_2, k_3 and k_4 represent the weights of different dimensions, and engineers can adjust the weights according to the actual needs to obtain a suitable path. m(n) represents the cost function of the roughness of the runner surface. In this paper, we processed the pipe with different forming angles by SLM technology and measured the roughness of its inner surface, as shown in Fig. 5. An expression for the surface roughness Ra can be obtained by fitting the results, which can then be used as an expression for M(n) as shown in Equation 5.

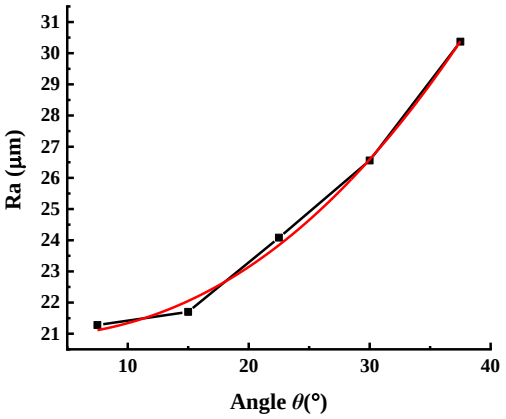

Figure 5 – Relationship between surface roughness Ra and angle θ.

$$M(\mathrm{n})=20.8714+0.0025 \bullet \theta_n^{\,2.2775} \tag{5}$$

Where θ_n is defined as the angle between the line connecting the two nodes of n and n-1 and the vertical direction. The goodness of fit is R^2 = 0.99263. The cost function R(n) is the resistance coefficient of the runner. Liu et al. [11] established a local resistance coefficient prediction model for

3D printing shaped piping, as shown in Eq. 6. The model is applicable to 90° bends, but the optimisation of the flow channel arrangement necessitates consideration of bends with different bending angles. Consequently, this model is further modified in this paper when establishing the R(n) expression, as shown in Equation 7.

$$\begin{cases} \zeta = k_{D/\mathrm{r}} \bullet k_{\mathrm{Re}} \bullet k_{\Delta/D} \\ k_{D/r} = 0.163 + 0.083 \bullet \left(\dfrac{D}{r}\right)^{4.149} \\ k_{\mathrm{Re}} = \begin{cases} 0.601 + 3819.873 \bullet \mathrm{Re}^{-1.093}, \mathrm{Re} \le 5000 \\ 1, \mathrm{Re} > 5000 \end{cases} \\ k_{\Delta/D} = \begin{cases} 4.981 - 1.371 \bullet \lg(\mathrm{Re}), \mathrm{Re} \le 586.025 + 9.711 \times 10^{14} \bullet \exp(-\dfrac{\Delta}{D \bullet 6 \times 10^{-5}}) \\ -28.746 + 2.154 \bullet 10^{-4} \bullet \mathrm{Re} + 3.467 \bullet 10^{-2} \bullet \lg(\mathrm{Re}) + 31041.133 \bullet \dfrac{\Delta}{D} - 8.102 \bullet 10^{6} \bullet \left(\dfrac{\Delta}{D}\right)^{2} \\ ,586.025 + 9.711 \times 10^{14} \bullet \exp(-\dfrac{\Delta}{D \bullet 6 \times 10^{-5}}) < \mathrm{Re} \le 3469.57 + 1.154 \times 10^{20} \bullet \exp(-\dfrac{\Delta}{D \bullet 4 \times 10^{-5}}) \\ 1.973 - 5918.617 \bullet \exp(-\dfrac{\Delta}{D \bullet 1.773} \bullet 10^{4}), \mathrm{Re} > 3469.57 + 1.154 \times 10^{20} \bullet \exp(-\dfrac{\Delta}{D \bullet 4 \times 10^{-5}}) \end{cases} \end{cases} \tag{6}$$

Where ζ is the local drag coefficient for a 90° bend, D is the inner diameter of the line, r is the turning radius, Re is the Reynolds number, and Δ/D is the relative average roughness.

$$R(n) = \frac{2\alpha_n}{\pi} \bullet \zeta \tag{7}$$

where α_n is the angle between the line connecting node n to node n-1 and the line connecting node n to node n+1.

4. Results and discussion

4.1 Simulation environment and optimisation process

In this paper, simulations are carried out using MATLAB R2019b software on a computer with operating system Windows 11, 16 GB RAM, Intel(R) Core(TM) i9-12900H 2.50 GHz. The component that has been optimised in this paper is the aero-hydraulic integrated block, as described in Section 2. As illustrated in Fig. 1, the hydraulic integrated block comprises multiple flow paths, each marked by a distinct colour. In this paper, the optimisation process is conducted by optimising each runner in accordance with its length, from longest to shortest. Additionally, given that each runner interfaces with multiple external components, the path is initiated from multiple points, necessitating the generation of multiple optimisations. In this paper, the main flow path is first optimised to generate the main flow path, and then the branch paths are optimised according to the distance between the external interface of the branch path and the main flow path, in the order from longest to shortest. When performing the alignment optimisation of the branch paths, it is necessary to identify a node on the main flow path as the target point of the branch path. In this study, the external interface of the branch road is taken as the starting point of the branch road, and the point on the main stream road with the smallest branch angle (the branch angle is the angle between the branch road and the main stream road) after connecting with the starting point is set as the target point of the branch road. The specific optimisation process is illustrated in Figure 6. The spatial map is populated with a grid of 10mm spacing, with the obstacle influence range set to 1.5.

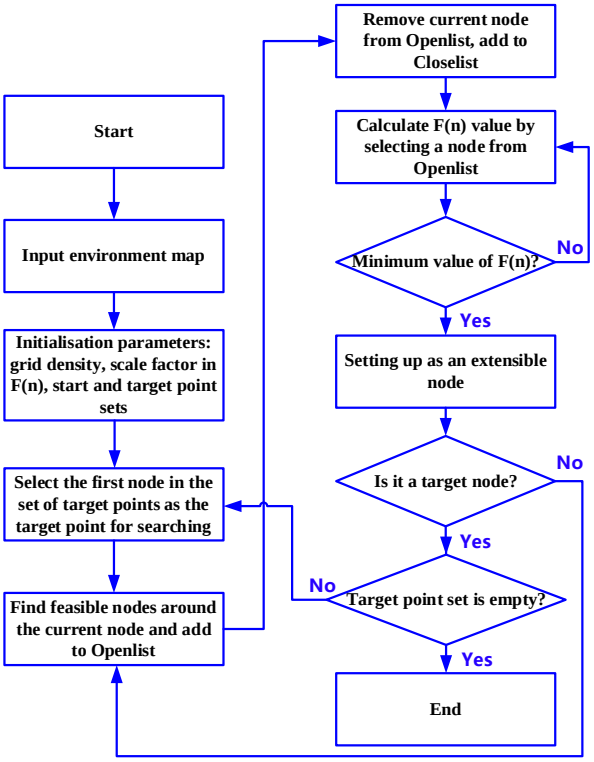

Figure 6 – Flowchart for optimisation of pipe arrangement in hydraulic manifolds.

4.2 Analysis of optimisation results

In this paper, the internal flow path of an aircraft hydraulic manifold (as shown in figure 1) is optimised using the improved A-star algorithm. The optimised pipeline centreline is shown in Fig. 7. The internal diameter of the pipes within the manifold is 4mm at each position. The pipes can be generated in Solidworks 2020 software according to the coordinates of the optimised pipe centreline and the pipe diameter, as shown in figure 8. As can be seen from the figure, this method can not only greatly reduce the length of the runner, but also effectively avoid the generation of additional structures such as blind cavities and process holes.

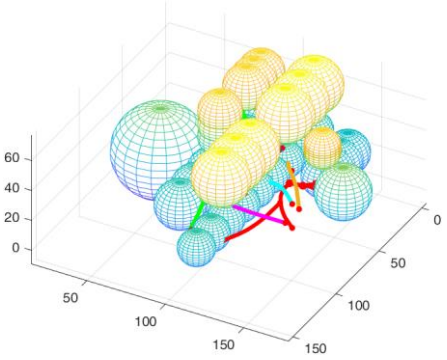

Figure 7 – Pipe centreline path optimisation.

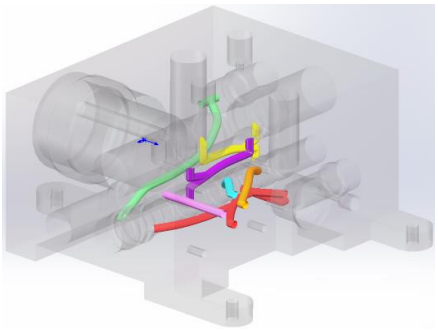

Figure 8 – Aircraft hydraulic manifold with optimised piping structure.

Furthermore, this paper presents a flow resistance simulation analysis of the optimised piping structure to evaluate the drag reduction effect of the A* algorithm on the piping. Given the multitude of pipelines in the hydraulic manifold, two representative internal flow paths containing right-angle turning pipelines, multiple inlets and multiple outlets are selected for this study. These flow paths are then simulated using the COMSOL finite element software to assess their respective flow resistance. In the analysis conducted using COMSOL simulation software, the fluid medium was set to be No. 15 aviation hydraulic oil with a density of 860 kg/m^3 and a dynamic viscosity of 0.0216 Pa·s at 40℃. The velocity inlet and pressure outlet were set, with the inlet velocity set to be 10 m/s and the outlet pressure set to be standard atmospheric pressure. The wall of the pipe is treated using the wall function. A standard k-ε turbulence model was employed for the calculations, with a turbulence intensity of 5% and a turbulence length of 7×10^{-4} m. Figure 9 illustrates the pressure distributions of two internal typical pipelines before and after the optimisation of the aircraft hydraulic manifold. As illustrated in Figure 9, the pressure loss of pipe 1 prior to optimisation was 293,218.96 Pa, while the pressure loss of pipe 1 following optimisation was 110,855.49 Pa, which indicates that the alignment optimisation method reduced the flow resistance of pipe 1 by 62.19%. Furthermore, the pressure loss of pipeline 2 before optimisation was 184831.16 Pa, while the pressure loss after optimisation was 56204.89 Pa, which demonstrates that the alignment optimisation method reduced the flow resistance of pipeline 2 by 69.59%.

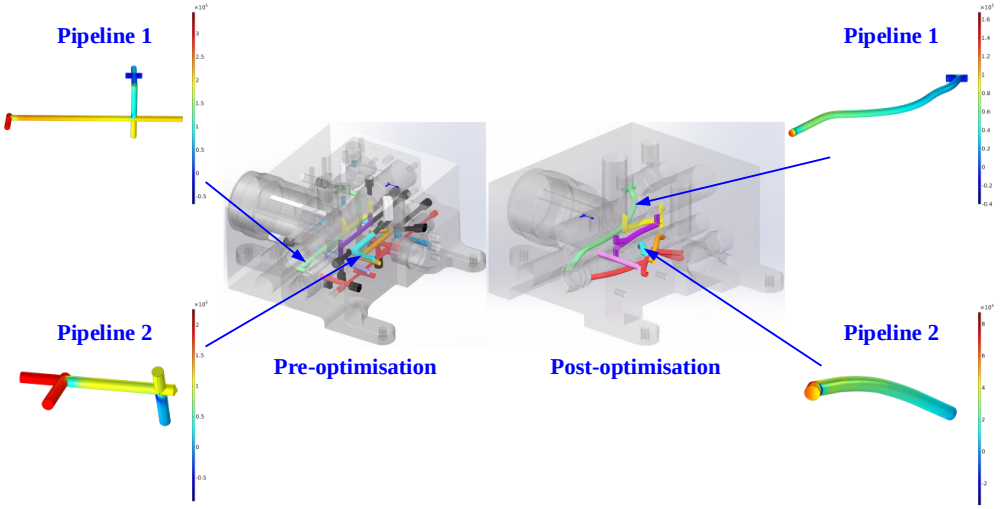

Figure 9 – Pressure distribution diagram for typical pipelines.

5. Conclusions

This paper presents a novel optimisation method based on the A-star algorithm for optimising the arrangement of flow paths within an L-PBF hydraulic manifold. The method is capable of achieving comprehensive optimisation of multi-directional runners in three dimensions, encompassing length, local resistance and forming quality. Additionally, it can be employed to arrange piping networks comprising multiple inlets and outlets in series. The method requires the input of obstacles in advance, after which the proportionality coefficients of runner length, local resistance and forming quality can be adjusted according to the needs of the actual project. This allows for the optimisation of any pipeline layout in the spatial network.This paper presents the application of an optimisation method to the design of the internal piping of an aircraft hydraulic manifold. The results demonstrate that the optimisation method is effective in removing additional structures, such as blind cavities and process holes, while also reducing pressure loss. Two representative pipelines within a hydraulic manifold are employed as case studies for simulation analysis in this paper. The results demonstrate that the flow path pressure losses are reduced by 62.19% and 69.59%, respectively.

6. Acknowledgements

This study was financially supported by the National Natural Science Foundation of China (Grant

No. 52205045), the National Key Research and Development Program of China (Grant No. 2021YFB2011300), the Aeronautical Science Foundation of China (Grant No.2022Z029051001), the Zhejiang Provincial Natural Science Foundation of China (Grant No. LZ24E050006), and the Academic Excellence Foundation of BUAA for PhD Students.

7. Contact Author Email Address

Xiaochao Liu: liuxiaochaoustb@163.com

8. Copyright Statement

References

[1] D. Thomas, The development of design rules for selective laser melting, Ph.D. thesis, University of Wales (2010).

[2] Zhu Y, Zhou L, Wang S, et al. On Friction Factor of Fluid Channels Fabricated using Selective Laser Melting[J]. Virtual and Physical Prototyping, 2020, 15(4): 496-509.

[3] Materials Solutions [EB/OL]. [2023-01-09]. https://materialssolutions.co.uk/.

[4] Sher D. First 3D Printed Hydraulic Manifold Successfully Flies on Airbus A380 Aircraft [EB/OL]. [2021-01-25]. http://www.3ders.org/.

[5] Yongtao H, Jingying M. A knowledge-based auto-reasoning methodology in hole-machining process planning[J]. Computers in Industry, 2006, 57(4):297-304.

[6] Woodwark J R. Solid Modelling of Fluid Power Components. Computer Aided Design in HighPressure Hydraulic Systems.1983.

[7] Chambon R, Tollenaere M. Automated AI-based mechanical design of hydraulic manifold blocks.Computer Aided Design,1991,23(3):213-222.

[8] Zardin B, Cillo G, Rinaldini C, et al. Pressure losses in hydraulic manifolds[J]. Energies, 2017, 10(1).

[9] Osamu Abe,Tetsuhiro Tsukiji,Takeshi Hara,and Kazutoshi Yasunaga. Flow analysis in pipe of a manifold block[J]. International Journal of Automation Technology,2012,6(4).

[10]Cooper D E, Stanford M, Kibble K A, et al. Additive Manufacturing for product improvement at Red Bull Technology[J]. Materials & Design, 2012, 41:226–230.

[11]Liu X, Li D, Qi P, et al. A local resistance coefficient model of aircraft hydraulics bent pipe using laser powder bed fusion additive manufacturing[J]. Experimental Thermal and Fluid Science, 2023, 147: 110961.